Dispersion-Mitigated Variance Reduction in Delay Times and Delay Lengths for Liquid Crystal-Based Variable Delay Lines from 54 GHz to 66 GHz and Beyond

Jinfeng Li,*[1,2,3,4] and Haorong Li[2]

[1]*School of Interdisciplinary Science, Beijing Institute of Technology, Beijing, 100081, China,*
[2]*Beijing Key Laboratory of Millimetre Wave and Terahertz, Beijing Institute of Technology, Beijing, 100081, China,*
[3]*Key Laboratory of Short-Range Radio Equipment Testing, Beijing Institute of Technology, Zhuhai, 519088, China,*
[4]*Electrical and Electronic Engineering Department, Imperial College London, London SW7 2AZ, United Kingdom*

Received June 27, 2025; accepted September 30, 2025; published September 30, 2025

Abstract—Since its inception three decades ago, liquid crystal (LC) microwave phase-shifting technology has made tangible and highly scalable improvements. Although LC-enabled phase shifts (measured in degrees or radians) have arguably produced a wealth of discoveries, delay length and delay duration (measured in picoseconds) have perhaps garnered significantly less attention. In this work, we numerically characterize the delay times and lengths of various LC-enabled variable delay line designs at the 60 GHz band, identifying the optimal dielectric constant state (baseline) that achieves a 50-ohm match while minimizing spikes and turbulence in the frequency response. In practice, the increase in the conventional figure-of-merit metric (i.e., the ratio of the maximum phase shift to the maximum insertion loss) has coincided with the ripples ramped up in the frequency response of the time delay. By suitably designing the geometry's matching baseline at the LC's permittivity state of 3.1, we achieve a quasi-constant delay time (and length) with minimised amplitude variations (standard deviation of 0.72 fs) across 54 GHz to 66 GHz, i.e., highly desirable for minimum squint and mitigated sidelobe for 60 GHz beam steering applications.

For wide bandwidth signals, conventional phase shifters cause a focusing-degraded phenomenon known as beam squint [1], in which distinct frequency components encounter varying temporal delays, obscuring signals and making them unintelligible. Various true-time delay techniques [2,3] have thus been introduced to circumvent this drawback. Among the hardware solution efforts, liquid crystals (LC) [4], with their unique electrically tunable dielectric/optical properties [5], offer a less conventional but intriguing avenue for manipulating signal delays continuously at microwave (delay lines) [6] or optical wavelengths (retarders) [7]. This analogue tunability is a crucial advantage in adapting to varying communication scenarios and optimizing signal integrity. The technical details of this, as outlined in existing documentation [8], are largely focused on the physics or material side, rather than engineering applications [9]. This work thus bridges the gap between the LC-based millimetre-wave (mmW) tunable transmission line design aspect and the beam steering application aspect, particularly for the 60 GHz band. More specifically, we propose to examine the relationship between delaying time and delaying length for time-domain beamforming using coaxial (non-planar) delay lines (see Fig. 1) with Merck GT3-24002 nematic LC across the 54 GHz to 66 GHz spectrum in terms of the maximum possible differential delay time and delay length with the least amount of frequency ripples (otherwise known as dispersion). Note that integrating ripple-free component design considerations and frequency ripple mitigation strategies into the early stages of the module-level design process is paramount compared to traditional approaches of addressing these issues at later system-level optimisation stages. The proactive design proposed for enhanced signal integrity is instrumental to prevent faulty operations (e.g., bit errors).

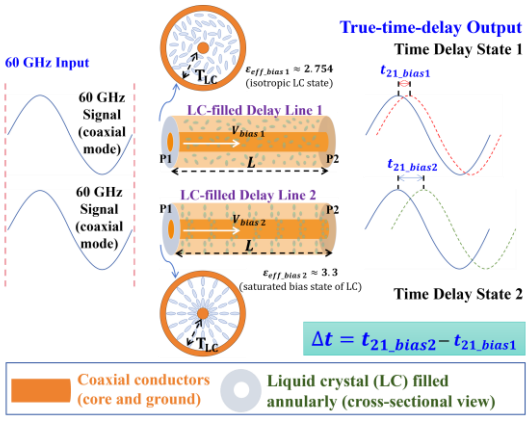

Fig. 1. Sketch of our coaxial solution of the LC variable delay line at 60 GHz, denoting the geometry of the LC thickness and th length of the device.

In our recent work [10] on the first LC-filled coaxial phase shifter, only the 60 GHz center-frequency response was characterized and optimized by loss decompositions.

* jinfengcambridge@bit.edu.cn

There remains a knowledge gap regarding the dispersion of the structure's effective dielectric constant (*Dk*) over frequency. The geometry was as per the optimised *FoM* design, with an LC thickness (T_{LC}) of 0.34876 mm, a core line diameter of 0.23 mm, and a line length (L) of 15.92 mm. The radial symmetry of the coaxial structure, however, introduces asymmetry in the LC's tuning capability away from the nematic phase, but entering an isotropic state, corresponding dielectrically to the LC's Dk_{iso} and the transmission line's minimum permittivity ($\varepsilon_{eff,min}$). The deviation from the saturated bias (corresponding to the LC's Dk_{sat}, i.e., device's maximum permittivity of $\varepsilon_{eff,max}$) gives rise to the maximally achievable phase shift (differential operation). Converting from the phase (degree) domain (Fig. 2) to the time domain by Eq. (1), the amount of differential delay time (Δt) produced by the *FoM*-optimised LC coaxial delay line design can be derived.

$$\Delta t = \frac{\Delta\Phi}{2\pi f} = \frac{L}{c}\left(\sqrt{\varepsilon_{eff,sat}} - \sqrt{\varepsilon_{eff,iso}}\right). \quad (1)$$

The differential delay length (ΔL) can subsequently be obtained by Eq. (2).

$$\Delta L = c\Delta t/\sqrt{\varepsilon_{eff}}. \quad (2)$$

Given that we take ε_{eff} based on the LC's *Dk* of 3.3 state, corresponding to *Dk* of 2.754 as the initial state and 3.3 as the ultimately biased state. The results of Δt and ΔL are shown in Fig. 3.

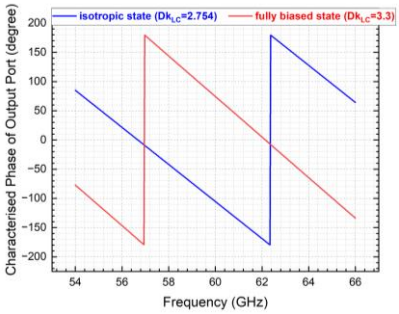

Fig. 2. Output phase characterised for the FoM-optimised LC-filled coaxial delay line. The deviation ΔΦ between the two curves constitutes.

In this work, a fleet of devices with diverse *Dk* baselines for impedance matching is trailed using the High-Frequency Structure Simulator (HFSS).
Characterised permittivity results are presented in Fig. 4 for different geometry designs (50-ohm matched at diverse *Dk* of LC). For differential delay length (ΔL), oscillation levels of various *Dk*-matching designs at the two extreme biasing statuses of LC are presented at Fig. 5 and Fig. 6, respectively.

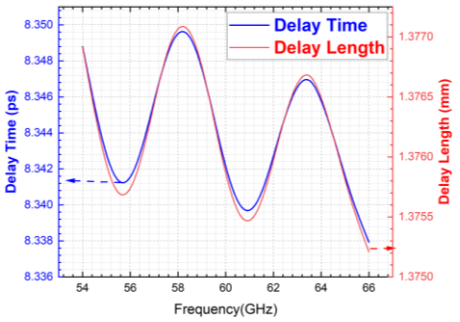

Fig. 3. Characterised results of Δt and ΔL based on LC's *Dk*=3.3 state.

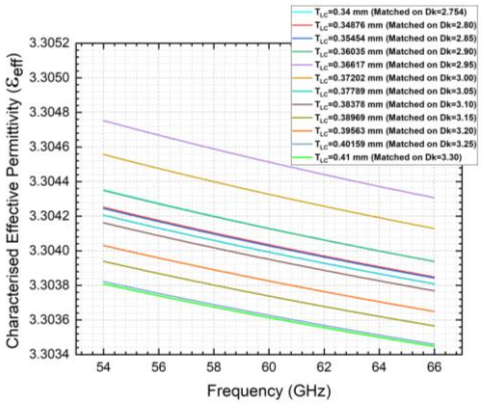

Fig. 4. Device's effective permittivity dispersion characterised for diverse *Dk*-match designs at LC's saturated state (i.e., LC's *Dk*=3.3).

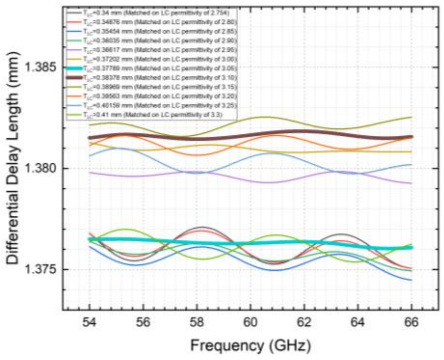

Fig. 5. ΔL characterised for various designs at the saturated bias state.

For enhanced resistance to defects in characterisations, statistical analysis is performed using a mean value and a standard deviation (SD). The post-analysis results, as per Fig. 7, the design matched at *Dk*=3.1 is subject to the smallest disturbances (SD of 0.72 fs) in the differential delay times versus frequency (from 54 GHz to 66 GHz).

The excellent anti-dispersion performance of the design (impedance matched at *Dk*=3.1) is also well evidenced in Figs. 5 and 6. Interestingly, this variance-mitigated design also exhibits the second-highest delay times and delay

lengths (desirable), i.e., the benefit of using this structure is two-fold.

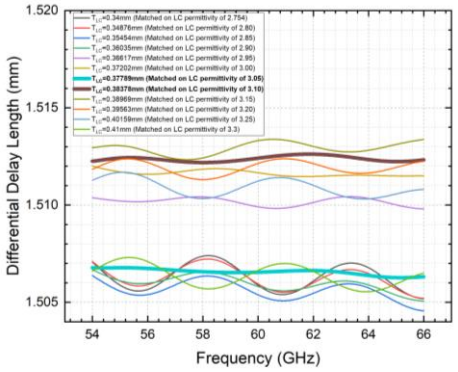

Fig. 6. ΔL characterised for various designs at the isotropic bias state.

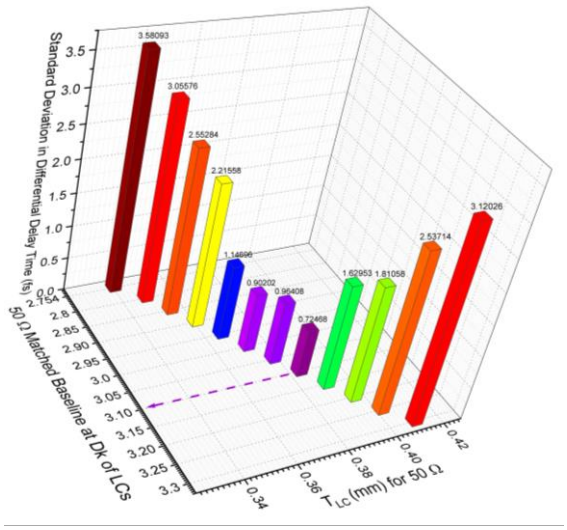

Fig. 7. Standard deviation (SD) of the characterised Δt vs. 50 Ω matched baseline of LC's tuning state (Dk) and the corresponding T_{LC}.

While this work illustrates decent improvements in dispersion-mitigated delay control for LC-based variable delay lines across 54 GHz to 66 GHz, further investigations are underway to extend these advancements to higher frequencies, e.g., systematic study of amplitude and phase ripples in LC-based variable delay lines at 300 GHz, with scaling laws to project performance toward sub-terahertz (sub-THz) and THz applications.

Future work will also focus on noise characterisation, e.g., quantifying the impact of thermal, shot, and hot electron noise [11, 12] on the delay precision, particularly in sub-THz and THz regimes where such noise mechanisms may dominate the performance limits. Furthermore, Smith Chart-based [13] analysis of the electrical length variation can be conducted at various tuning states of the LC to refine the impedance matching and minimize reflections across the spectrum. These efforts will bridge the gap of mmW and THz beamforming, enabling robust, wideband phased arrays for 5G/6G communications and sensing [14].

In conclusion, this work presents a liquid crystal-based true-time-delay solution with tuning-state-dependent impedance-matching baselines optimized to overcome the bottleneck of conventional phased arrays in high-frequency mmW beam scanning, which traditionally suffers from dispersion and unstable phase-shifting (time-delaying) accuracy.

More specifically, this work numerically indicates the possibility of variance reduction in the delay times and delay lengths of liquid crystal tunable delay lines, taking the spectrum from 54 GHz to 66 GHz (i.e., ±10% of the center frequency of 60 GHz) as an example. Among a host of geometry designs, this work bridges the knowledge gap in understanding how these frequency fluctuations occur by parameterising the permittivity-dependent 50-ohm impedance-matching baseline for improved flatness of the variable delay times and lengths in the frequency response across 54 GHz to 66 GHz. The results and implications are envisioned to address the formidable dispersion challenge of beam steering and tracking in the high-frequency mmW regime, a significant milestone of 5G and beyond.

This study is supported by the National Natural Science Foundation of China (NSFC Grant 62301043), as well as the Beijing Institute of Technology Research Fund Programme for Young Scholars.

References

[1] M. Dasan, S. Vidyamol, P.A. Prasad, IEEE Microwaves, Antennas, and Propagation Conference (Hyderabad, IEEE 2024). doi: 10.1109/MAPCON61407.2024.10923018
[2] R. Rotman, M. Tur, L. Yaron, Proc. IEEE **104**, 3 (2016). doi: 10.1109/JPROC.2016.2515122
[3] E. Kim, I. Kim, S. Han, *et al.,* Remote Sensing **14**, 18 (2022). doi: 10.3390/rs14184489
[4] V. Sultanov, A. Kavčič, E. Kokkinakis, N. Sebastián, M.V. Chekhova, M. Humar, Nature **631**, 294 (2024). doi: 10.1038/s41586-024-07543-5
[5] J. Guardià, J. A. Reina, M. Giamberini, X. Montané, Polymers **16**, 16 (2024). doi: 10.3390/polym16162293
[6] J.F. Li, Proc. SPIE **12764**, 127640X (2023). doi: 10.1117/12.2685859
[7] A. Jullien, U. Bortolozzo, S. Grabielle, J. Huignard, N. Forget, S. Residori, Optics Expr. **24**, 13 (2016). doi: 10.1364/OE.24.014483
[8] S. Kumar, Molecules **6**, 1055 (2001). doi: 10.3390/61201055
[9] J.F. Li, D.P. Chu, Crystals **9**, 12 (2019). doi: 10.3390/cryst9120650
[10] J.F. Li, H.R. Li, Electronics **13**, 3 (2024). doi: 10.3390/electronics13030626
[11] E. Šermukšnis, A. Šimukovič, V. Avrutin, N. Izyumskaya, Ü. Özgür, H. Morkoç, Crystals **14**, 75 (2024). doi: 10.3390/cryst14010075
[12] E. Sivre, H. Duprez, et al., Nature Comm. **10**, 5638 (2019). doi: 10.1038/s41467-019-13566-8
[13] E.F. A. Malaver, N.B. Lombana, J.J. M. Rubio, Electronics **13**, 20 (2024). doi: 10.3390/electronics13204096
[14] A. Govind, T. Tapen, A. Apsel, Nature **627**, 88 (2024). doi: 10.1038/s41586-024-07075-y